Virtual element method for computational homogenization of composite and heterogeneous materials

Marco Lo Cascio[a], Alberto Milazzo[a], Ivano Benedetti[a,*]

[a]*Department of Engineering, University of Palermo, Viale delle Scienze, Edificio 8, Palermo, 90128, Italy.*

Abstract

In this study, a two-dimensional multi-region framework, based on the use of the Virtual Element Method (VEM), is developed for computational materials homogenization and applied to different classes of widely employed heterogeneous materials. The VEM has recently emerged as a powerful generalisation of the Finite Element Method capable of dealing with very general polygonal mesh elements, including non-convex or highly distorted elements. Such features are appealing for the treatment of problems whose analysis domains present complex or statistical morphological features, which would generally require careful and time-consuming mesh/data preparation and regularization. In this work, the lowest-order VEM for two-dimensional elastostatics is employed for the homogenization of polycrystalline materials and unidirectional fibre-reinforced composites. In both cases, artificial micro-morphologies are usually generated resorting to automatic algorithms aimed at approximating/reproducing the statistical microscopic features of real materials. In such a context, the likely presence of morphological irregularities, and subsequent mesh distortions, usually requires caution and the employment of sophisticated mesh regularization procedures. The study demonstrates how the inherent features of the VEM can be conveniently exploited for such classes of problems, as the method allows the relaxation of the requirements on the mesh quality, yet providing accurate numerical results.

Keywords: Micromechanics, Computational homogenization, Composite materials, polycrystalline materials, Virtual element method

*Corresponding author

Email addresses: marco.locascio01@unipa.it (Marco Lo Cascio), alberto.milazzo@unipa.it (Alberto Milazzo), ivano.benedetti@unipa.it (Ivano Benedetti)

1. Introduction

The properties of a material at a certain scale depend on the features of and mutual interactions among the material constituents at lower scales [1]. The ability to understand, explain and predict macroscopic material properties from a suitable description of the micro-scale is of relevant technological interest, especially in connection with the contemporary availability of manufacturing technologies offering a tighter control on the materials microstructure.

Computational micro-mechanics has emerged as a consistent framework supporting the understanding of the link between the material microstructure and its macroscopic properties, i.e. the *structure-property relationship* [2]. The field has enormously benefitted from the rapid advancements of experimental techniques for materials microscopic characterization and reconstruction, able to provide a wealth of useful processable information, and from the increased affordability of high performance computing (HPC), which provide the complementary ability of combining and processing such information towards better understanding, prediction and manipulation.

Polycrystalline materials and fibre-reinforced composites are two classes of materials widely employed in engineering applications. In polycrystalline materials, the availability of information about the mechanical properties of the grains and their inter-granular interfaces, their crystallographic orientation and size distribution can be conveniently exploited to predict the properties of the aggregate and suggest potential manufacturing pathways for material optimization [3, 4, 5]. Analogously, the knowledge of the properties of carbon fibres, epoxy matrix and the characterisation of the fibre-matrix interface can be used to investigate the effectiveness of different fibre arrangements on the structural performances of composite laminates [6, 7].

It is apparent how the computational capability of predicting the effect of microstructural parameters on the macro-properties has direct technological implications, contributing to reducing the cost of experimental campaigns for the design of new materials. In the ambitious paradigm known as *materials-by-design*, the much sought-after capability of modelling materials *ab initio*, i.e. starting from the smallest nano-scales, exploiting first principles, such as quantum mechanics, should enable the design of materials with properties tailored to specific applications.

In this paper, attention is focused on *continuum* micro-mechanics, i.e. on the study of materials whose basic building blocks, e.g. individual crystals, fibres or matrix, can be modelled resorting to the continuum idealisation. In this framework, several numerical methods have been used to investigate the structure-property link. The finite element method (FEM) is the most popular approach

and it has been extensively used to investigate several kinds of materials, including polycrystalline [3, 8, 9] and composite materials [10, 11, 12]. Other techniques have also been used, including the extended finite element method (X-FEM) [13, 14], the boundary element method [15, 16, 17, 18], meshfree methods [19, 20] among others.

One of the key aspects in the effective modelling of materials micro-mechanics is the availability of a suitable representation of the material micro-morphology, which may exhibit involved shapes. The potential presence of complex morphological features has a direct effect on the complexity of the numerical grid, or mesh, used to discretise the considered boundary value problem. The quality of the mesh, in turn, may have an important effect on the accuracy of the numerical reconstruction of the mechanical fields. Indeed, the preparation of high-quality meshes is today one of the steps requiring more attention, and time, from the analyst [21, 22].

The *Virtual Element Method* (VEM) was recently introduced [23, 24] as generalisation of the FEM and applied to general linear elasticity [25, 26, 27], inelastic materials at small strains [28, 29], hyper-elastic materials at finite strains [30, 31], contact mechanics [32], topology optimization [33, 34], magneto-static problems [35, 36], geomechanical simulations of reservoir models [37], fracture analysis [38, 39] and plate bending problems [40, 41] and materials homogenization of heterogeneous materials [42, 43, 44, 45, 46].

Some remarkable features of the VEM are related to its ability to deal with mesh elements of very general polygonal/polyhedral shape and to naturally address the presence of hanging nodes, providing accurate and consistent analysis results even with heavily distorted meshes. Such flexibility makes the VEM an ideal candidate tool for computational homogenization studies, where the structure-property link is investigated homogenising the micro-fields over several statistical realisations of the material microstructure; in other words, being computational homogenization based on the analysis carried out over many micro representative volume elements, often generated and meshed automatically, the possibility to relieve the need of carefully assessing the quality of *each* mesh, makes the VEM a suitable method for such analysis.

In this paper, the application of the VEM to the computational homogenization of polycrystalline and fibre-reinforced materials is reported. Emphasis is given to the flexibility given by the method in the analysis of randomly generated and meshed microstructures. The paper is organised as follows. Section 2 briefly reviews the fundamentals of VEM. Section 3 details some computational aspects implemented to deal with generic polycrystalline and fibre-reinforced micro-morphologies

and their meshing, describing the suitability of the method in dealing with specific features. Section 4 illustrates the application of the method to the computational homogenization of the considered materials and concludes the study.

2. VEM for 2D linear elastostatics

The Virtual Element Method is a generalization of the Finite Element Method to general polygonal/polyhedral meshes and, in this respect, it shows some similarities with other polygonal/polyhedral finite element methods [47]. In the VEM the trial and test functions over each mesh element belong to a space containing all the polynomials up to a certain previously selected order k plus other additional functions that, in general, are not polynomials and are solutions, within the element, of a suitably defined boundary value problem. Such additional functions are explicitly known only over the element edges while, within each element, they are not explicitly known and never computed, which justifies the adjective *virtual* referred to the method. Once such a local functional basis is selected, the discrete counterpart of the local bilinear form and of the linear functionals in the variational formulation can be computed by expressing the virtual trial and test functions through their polynomial projections. Through a particular choice of the element degrees of freedom, such projections are exactly computed as a function of the degrees of freedom themselves, without actually solving the local boundary value problem.

2.1. Weak form for 2D linear elasticity

Two-dimensional elasticity problems at small strains are considered in this work. An elastic body lying within the polygonal domain $\Omega \subset \mathbb{R}^2$ bounded by the curve $\Gamma = \partial\Omega$ is considered. In general, the body is subjected to a distributed volume load $\boldsymbol{f}(\boldsymbol{x})$, where $\boldsymbol{x} \in \mathbb{R}^2$ denotes the coordinates of a generic point in the two-dimensional space. Without loss of generality and for a more concise explanation, homogeneous boundary conditions are assumed; however other types of boundary conditions can be enforced following the same procedures as those used for the standard finite element method.

The strong formulation of the 2D elasto-static problem is based on the use of the strain-displacement equations

$$\boldsymbol{\varepsilon}(\boldsymbol{u}) = \boldsymbol{\mathcal{S}}\boldsymbol{u}, \tag{1}$$

the linear elastic constitutive laws

$$\boldsymbol{\sigma} = \boldsymbol{C}\boldsymbol{\varepsilon}, \tag{2}$$

and the indefinite equilibrium equations

$$\boldsymbol{\mathcal{S}}^T\boldsymbol{\sigma} + \boldsymbol{f} = \boldsymbol{0}, \tag{3}$$

where $\boldsymbol{u}(\boldsymbol{x})$ represents the displacement vector field, $\boldsymbol{\varepsilon}(\boldsymbol{u})$ is the strain tensor field in Voigt notation, $\boldsymbol{\sigma}$ is the stress tensor field in Voigt notation, $\boldsymbol{C} = \boldsymbol{C}(\boldsymbol{x})$ represents the stiffness tensor in Voigt notation and

$$\boldsymbol{\mathcal{S}} = \begin{bmatrix} \partial_x & 0 \\ 0 & \partial_y \\ \partial_y & \partial_x \end{bmatrix} \tag{4}$$

represents the small-strains linear differential matrix operator, with $\partial_x = \partial(\cdot)/\partial x$ and $\partial_y = \partial(\cdot)/\partial y$.

The weak formulation of the considered problem, derived from the principle of virtual displacements, consists in searching the solution displacements field $\mathbf{u}(\boldsymbol{x}) \in \boldsymbol{V} := \left[H_0^1(\Omega)\right]^2$ such that

$$a(\boldsymbol{u}, \boldsymbol{v}) = \mathcal{L}(\boldsymbol{v}) \quad \forall \boldsymbol{v}(\boldsymbol{x}) \in \boldsymbol{V}, \tag{5}$$

where $\boldsymbol{V}$ is the space of kinematically admissible displacements and $H_0^1(\Omega)$ is the first order Sobolev space, defined on Ω, consisting of square integrable scalar functions with square integrable first derivatives and vanishing on Γ. In Eq.(5), the symmetric bilinear form $a(\cdot,\cdot)$ can be associated to the strain energy stored in the body and it is defined as

$$a(\boldsymbol{u}, \boldsymbol{v}) := \int_\Omega \boldsymbol{\varepsilon}(\boldsymbol{v})^{\mathrm{T}} \boldsymbol{C}\boldsymbol{\varepsilon}(\boldsymbol{u})\, d\Omega \tag{6}$$

while the linear functional $\mathcal{L}(\cdot)$ can be associated to the the virtual work of the volume load and it is defined as

$$\mathcal{L}(\boldsymbol{v}) := \int_\Omega \boldsymbol{v}^{\mathrm{T}} \boldsymbol{f}\, d\Omega \tag{7}$$

To obtain an approximate solution to the boundary-value problem based upon the weak formulation in Eq.(5), the domain Ω is sub-divided into a collection Ω_h of finite non-overlapping elements $E \in \Omega_h$, interconnected at nodal points on the boundary of each element. Once the domain discretization Ω_h is established, a function space $\boldsymbol{V}_h \subset \boldsymbol{V}$, which is a finite-dimensional approximation

of $\boldsymbol{V}$, is associated to it. The Galerkin formulation of the problem in hand consists in finding an approximate weak solution $\boldsymbol{u}_h \in \boldsymbol{V}_h$ such that

$$a(\boldsymbol{u}_h, \boldsymbol{v}_h) = \mathcal{L}\left(\boldsymbol{v}_h\right) \quad \forall \boldsymbol{v}_h \ \in \boldsymbol{V}_h \tag{8}$$

Both sides of Eq.(8) can be split into elemental contributions $a_E(\cdot,\cdot)$ and $\mathcal{L}_E(\cdot)$, i.e.

$$a(\boldsymbol{u}_h, \boldsymbol{v}_h) = \sum_{E\in\Omega_h} a_E(\boldsymbol{u}_h, \boldsymbol{v}_h) = \sum_{E\in\Omega_h} \int_E \boldsymbol{\varepsilon}(\boldsymbol{v}_h)^{\mathrm{T}} \boldsymbol{C} \boldsymbol{\varepsilon}(\boldsymbol{u}_h)\, dE \tag{9}$$

and

$$\mathcal{L}\left(\boldsymbol{v}_h\right) = \sum_{E\in\Omega_h} \mathcal{L}_E\left(\boldsymbol{v}_h\right) = \sum_{E\in\Omega_h} \int_E \boldsymbol{v}_h^{\mathrm{T}} \boldsymbol{f}\, dE \tag{10}$$

2.2. Virtual Element formulation

In this section, the first-order virtual element formulation used to find an approximate solution to the problem presented in Eq.(8) is reviewed. The discretization Ω_h of the two-dimensional domain Ω consists in a collection of non-overlapping polygonal elements interconnected at nodal points on the elements boundaries. The VEM allows to choose elements with very general shapes, including non-convex polygons, and with an arbitrary number of edges. In the following, for each element E, $\boldsymbol{x}_E$, h_E and $|E|$ denote the centroid, the diameter and the area of E, respectively. The element boundary is denoted by ∂E and $\boldsymbol{n}_E$ is the unit normal vector to ∂E. Finally, the symbols v_i $(i = 1, 2..., m)$ will indicate the counter-clockwise ordered vertices of E and e_i $(i = 1, 2..., m)$ will refer to the edge having v_i as its first vertex (see Fig.(1)).

For each element E, the local discrete virtual space of admissible displacements is defined as in Ref.[25], i.e.

$$\begin{aligned} \boldsymbol{V}_h(E) := \Big\{ \boldsymbol{v}_h \in \left[H^1(E) \cap C^0(E)\right]^2 : \boldsymbol{v}_{h|\partial E} \in \left[C^0(\partial E)\right]^2, \\ \boldsymbol{v}_{h|e} \in \left[P_1(E)\right]^2, \ \forall e \in \partial E, \ \mathcal{S}^{\mathrm{T}} \boldsymbol{C} \boldsymbol{\varepsilon}(\boldsymbol{v}_h) = \boldsymbol{0} \text{ in } E \Big\} \end{aligned} \tag{11}$$

where $P_k(E)$ is the space of polynomials of degree k on E. The global discrete virtual space is obtained by assembling all the local spaces $\boldsymbol{V}_h(E)$

$$\boldsymbol{V}_h := \left\{ \boldsymbol{v}_h \in \boldsymbol{V} : \boldsymbol{v}_{h|E} \in \boldsymbol{V}_h(E) \quad \forall E \in \Omega_h \right\}. \tag{12}$$

For the first-order VEM here considered, the degrees of freedom are the point-wise values of $\boldsymbol{v}_h$ at each vertex v_i of E. It should be observed that, differently from the classical FEM, the explicit

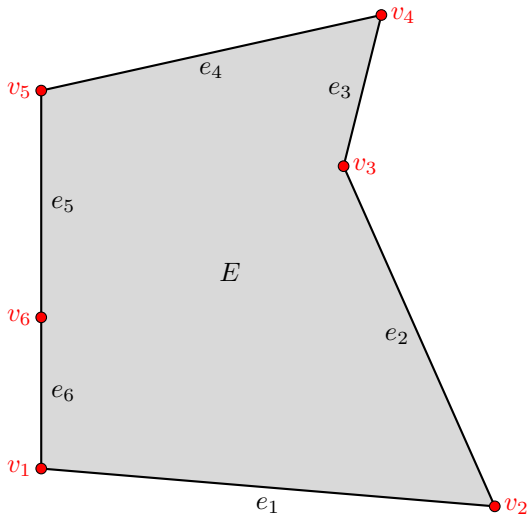

Fig. 1. Example of a non-convex VEM element with hanging nodes.

knowledge of the functions $\boldsymbol{v}_h$ of the space $\boldsymbol{V}_h(E)$ is not required over the whole element domain, thus explaining the adjective *virtual*. In fact, $\boldsymbol{V}_h(E)$ is made of vector-valued functions $\boldsymbol{v}_h$ that are explicitly known only on the element boundary ∂E, where they are globally continuous and, in the case of the first order VEM, they are linear polynomials on each edge e_i of E. Due to the fact that the functions of $\boldsymbol{V}_h$ are not explicitly known within the domain of the element E, the local discrete bilinear form $a_E(\cdot,\cdot)$ cannot be computed by standard numerical integration, as usually done in classical FEM. In order to overcome this issue, the VEM approach is based on the use of a projector operator Π, defined on each element E by the following orthogonality condition

$$\int_E \boldsymbol{p}^{\mathrm{T}} \left[\Pi(\boldsymbol{v}_h) - \boldsymbol{\varepsilon}(\boldsymbol{v}_h)\right] dE = 0 \quad \forall \boldsymbol{p} \in \left[P_0(E)\right]^3 \tag{13}$$

where $\Pi(\boldsymbol{v}_h)$ are the approximated strains associated with the displacements field, assumed to be constant in each element E in the case of first-order approximation. Since $\boldsymbol{p}$ has constant components as well, Eq.(13) may be written as

$$\Pi(\boldsymbol{v}_h) = \frac{1}{|E|} \int_E \boldsymbol{\varepsilon}(\boldsymbol{v}_h)\, dE. \tag{14}$$

Analogously to what done in FEM, each function $\boldsymbol{v}_h \in \boldsymbol{V}_h(E)$ can be expressed as

$$\boldsymbol{v}_h = \boldsymbol{N}\, \tilde{\boldsymbol{v}} \tag{15}$$

where

$$\boldsymbol{N} = \begin{bmatrix} N_1 & 0 & N_2 & 0 & ... & N_m & 0 \\ 0 & N_1 & 0 & N_2 & 0 & ... & N_m \end{bmatrix} \tag{16}$$

is the matrix containing the *virtual* shape functions $N_i(\xi, \eta)$ (never explicitly represented within the element domain) associated with each node i of the element E and

$$\tilde{\boldsymbol{v}} = \begin{bmatrix} \tilde{v}_{x1} & \tilde{v}_{y1} & \tilde{v}_{x2} & \tilde{v}_{y2} & ... & \tilde{v}_{xm} & \tilde{v}_{ym} \end{bmatrix}^{\mathrm{T}} \tag{17}$$

is the vector collecting the nodal values of $\boldsymbol{v}_h$. The projected strains can be expressed in terms of the nodal values of $\boldsymbol{v}_h$ as

$$\Pi(\boldsymbol{v}_h) = \boldsymbol{\Pi}\, \tilde{\boldsymbol{v}} \tag{18}$$

where $\boldsymbol{\Pi} \in \mathbb{R}^{3\times 2m}$ is the discrete representation of the local projector.

Taking into account Eq.(1), Eq.(14) and Eq.(15), Eq.(18) may be rewritten as

$$\boldsymbol{\Pi}\, \tilde{\boldsymbol{v}} = \frac{1}{|E|} \int_E \boldsymbol{\mathcal{S}} \boldsymbol{N} \tilde{\boldsymbol{v}}\, dE \tag{19}$$

By applying the Green's theorem to the right-hand side of Eq.(19), one gets

$$\boldsymbol{\Pi} = \frac{1}{|E|} \int_{\partial E} \boldsymbol{\mathcal{N}} \boldsymbol{N} ds = \frac{1}{|E|} \sum_{i=1}^{m} \int_{e_i} \boldsymbol{\mathcal{N}}_i \boldsymbol{N} ds \tag{20}$$

where

$$\boldsymbol{\mathcal{N}} = \begin{bmatrix} n_x & 0 \\ 0 & n_y \\ n_y & n_x \end{bmatrix} \tag{21}$$

is the matrix containing the components n_x and n_y of the outward unit vector $\boldsymbol{n} = \begin{bmatrix} n_x & n_y \end{bmatrix}^{\mathrm{T}}$ normal to the element boundary ∂E and $\boldsymbol{\mathcal{N}}_i$ is the matrix associated to the edge e_i. It should be noted that the boundary integrals on the right-hand side of Eq.(20) are exactly computable, since the restriction of the shape functions N_i to the element boundary edges are *known* piece-wise linear polynomials.

The VEM uses an approximation of the local symmetric bilinear form $a_E(\cdot, \cdot)$ that satisfies the *consistency* and *stability* properties (see Ref.[23]), defined, for all $E \in \Omega_h$ and for all $\boldsymbol{u}_h, \boldsymbol{v}_h \in \boldsymbol{V}_h$, as

$$a_{h,E}\left(\boldsymbol{u}_h, \boldsymbol{v}_h\right) = \int_E \left[\Pi(\boldsymbol{v}_h)\right]^{\mathrm{T}} \boldsymbol{C}\, \Pi(\boldsymbol{u}_h)\, dE + s_E\left(\boldsymbol{u}_h, \boldsymbol{v}_h\right). \tag{22}$$

The first term on the right-hand side of Eq.(22), referred to as the *consistency* term, ensures that if the solution of the original problem is, globally, a linear polynomial, then the solution of the discrete problem coincides with the exact solution. Using Eq.(18), it can be expressed as

$$\int_E \left[\Pi(\boldsymbol{v}_h)\right]^{\mathrm{T}} \boldsymbol{C}\, \Pi(\boldsymbol{u}_h)\, dE = \int_E \left[\boldsymbol{\Pi}\, \tilde{\boldsymbol{v}}\right]^{\mathrm{T}} \boldsymbol{C}\, \boldsymbol{\Pi}\, \tilde{\boldsymbol{u}}\, dE = \tilde{\boldsymbol{v}}^{\mathrm{T}} \left(\int_E \boldsymbol{\Pi}^{\mathrm{T}} \boldsymbol{C}\, \boldsymbol{\Pi}\, dE \right) \tilde{\boldsymbol{u}} = \tilde{\boldsymbol{v}}^{\mathrm{T}} \boldsymbol{K}_E^c\, \tilde{\boldsymbol{u}} \tag{23}$$

where

$$\boldsymbol{K}_E^c = |E|\, \boldsymbol{\Pi}^{\mathrm{T}} \boldsymbol{C}\, \boldsymbol{\Pi} \tag{24}$$

is the *consistency* contribution to the element stiffness matrix $\boldsymbol{K}_E$.

The second term on the right-hand side of Eq.(22) is referred to as the *stability* term and it is a symmetric bilinear form that ensures the proper rank of the element stiffness matrix $\boldsymbol{K}_E$. Following Ref.[27], to which the interested reader is referred for further details, the stability term may be written in matrix form as

$$s_E\left(\boldsymbol{u}_h, \boldsymbol{v}_h\right) = \tilde{\boldsymbol{v}}^{\mathrm{T}} \boldsymbol{K}_E^s\, \tilde{\boldsymbol{u}} \tag{25}$$

where $\boldsymbol{K}_E^s$ is the stability contribution to the element stiffness matrix, which can be expressed as

$$\boldsymbol{K}_E^s = \left[\boldsymbol{I} - \boldsymbol{\Pi}^s\right]^{\mathrm{T}} \mu\, \left[\boldsymbol{I} - \boldsymbol{\Pi}^s\right], \tag{26}$$

where $\boldsymbol{I} \in \mathbb{R}^{2m \times 2m}$ is the identity matrix and $\boldsymbol{\Pi}^s$ is a matrix projector operator that may be written as

$$\boldsymbol{\Pi}^s = \boldsymbol{D} \left(\boldsymbol{D}^{\mathrm{T}} \boldsymbol{D}\right)^{-1} \boldsymbol{D}^{\mathrm{T}} \tag{27}$$

where

$$\boldsymbol{D} = \begin{bmatrix} 1 & 0 & \xi_1 & 0 & \eta_1 & 0 \\ 0 & 1 & 0 & \xi_1 & 0 & \eta_1 \\ \vdots & \vdots & \vdots & \vdots & \vdots & \vdots \\ 1 & 0 & \xi_m & 0 & \eta_m & 0 \\ 0 & 1 & 0 & \xi_m & 0 & \eta_m \end{bmatrix} \tag{28}$$

and ξ_i and η_i, with $i = 1, ..., m$, are the *local scaled coordinates* of the vertices of element E, defined according to

$$\xi_i = \frac{x_i - x_E}{h_E}, \qquad \eta_i = \frac{y_i - y_E}{h_E}, \tag{29}$$

where it is recalled that (x_E, y_E) and h_E are the centroid coordinates and diameter, respectively, of the considered element. The coefficient $\mu = \tau\, \mathrm{tr}\left(\boldsymbol{K}_E^c\right)$ is a constant parameter that is used to ensure

the correct scaling of the stability term with respect to the element size and material constants. For linear elasticity problems, τ can be set equal to 0.5 (see Ref.[25]).

Eventually, for the lowest order VEM, the local contribution $\mathcal{L}_E(\cdot)$ to the virtual work of the volume load $\boldsymbol{f}$ that appears in the right-hand side of Eq.(8) can be approximated as in Ref.[23], i.e.

$$\mathcal{L}_E\left(\boldsymbol{v}_h\right) \approx \mathcal{L}_{h,E}\left(\boldsymbol{v}_h\right) = \int_E \bar{\boldsymbol{v}}_h^{\mathrm{T}} \boldsymbol{f}_h \, dE \tag{30}$$

where $\bar{\boldsymbol{v}}_h$ denotes the average value of $\boldsymbol{v}_h$ at the vertices of E, defined by

$$\bar{\boldsymbol{v}}_h = \frac{1}{m}\sum_{i=1}^{m} \boldsymbol{v}_h(\tilde{\boldsymbol{x}}_i) = \frac{1}{m}\sum_{i=1}^{m} \boldsymbol{N}(\tilde{\boldsymbol{x}}_i)\tilde{\boldsymbol{v}}, \tag{31}$$

and $\boldsymbol{f}_h$ is defined on each element E as the $L^2(E)$ projection onto constants of the load $\boldsymbol{f}$, i.e.

$$\boldsymbol{f}_h = \Pi_0\left(\boldsymbol{f}\right) := \frac{1}{|E|}\int_E \boldsymbol{f} \, dE. \tag{32}$$

It is worth noting that, since the shape functions N_i are explicitly known on the element boundaries, the enforcement of non-homogeneous boundary conditions can be done exactly as in standard FEM.

The element stiffness matrix $\boldsymbol{K}_E$ is obtained by summing the *consistency* term and the *stability* term defined in Eq.(24) and Eq.(26), respectively, thus giving

$$\boldsymbol{K}_E = \boldsymbol{K}_E^c + \boldsymbol{K}_E^s. \tag{33}$$

Eq.(32) and Eq.(33) provide the means to compute the local discrete equilibrium equations for the elasto-static problem within the framework of the lowest-order VEM, which can be written as

$$\boldsymbol{K}_E\tilde{\boldsymbol{u}} = \boldsymbol{f}_h. \tag{34}$$

Once the elemental matrices are built, the numbering, assembly and solution of the overall structural problem can be performed following standard FE procedures, which motivates the appeal of the VEM as a versatile method requiring minimum re-coding in existing software packages.

In the previous sections, the main advantages of VEM over standard FEM have been extensively stressed. However, it is worth underlining some differences in the computational implementation between the lowest-order VEM, adopted here, and the standard FEM. With respect to standard FEM elements of comparable numerical accuracy (e.g. Constant Strain Triangle - CST), the population of the VEM elemental stiffness matrix requires performing additional operations, due to the

computation of the stabilization term. More specifically, the construction of the stability projector $\boldsymbol{\Pi}^s$ requires the computation of the inverse of matrix $\boldsymbol{D}^{\mathrm{T}}\boldsymbol{D}$ in Eq.(27). However, given that the size of matrix $\boldsymbol{D}$ is proportional to the usually limited number of element edges, this operation is not *per se* computationally expensive, but it may increase the overall computational cost when the analysed model contains a large number of elements. It is stressed that such observations hold for the lowest-order VEM, employed here; the formulation and implementation of arbitrary order VEM involves more sophisticated considerations that go beyond the scope of the present study and form the object of much current research [24].

3. Multi-domain implementation for computational material homogenization

In this section, the multi-region implementation for computational material homogenization is described with reference to two classes of materials, namely polycrystalline and unidirectional fibre-reinforced composites, widely employed in engineering applications.

Some applications of the VEM to material homogenization of composites [42, 43, 45] and polycrystalline materials [46] have very recently appeared in the literature. Refs.[42, 43] consider unit cells with a single circular or elliptical inclusion, considered as the basic building block of composite materials with regular fibres distributions. Ref.[45] considers domains with a statistical distribution of fibres, but a single polygonal VEM element is used to model the individual fibres. Ref.[46] uses single polygonal or polyhedral VEM elements to model individual crystals in 2D and 3D, for homogenization purposes. In the present study, the focus is slightly different. Multi-domain microstructures obtained from random processes are considered and no *a priori* assumption is made about the number of VEM elements used to model individual fibres or crystals. Emphasis is given to the flexibility offered by the features of VEM in meshing such general morphologies, which make it a convenient method for the analysis of complex random material microstructures.

The first step toward materials computational micro-mechanics is the adoption of an accurate representation of the material microstructure. This can be based either on experimental reconstruction of real microstructures or on computer generation of artificial models embodying the relevant statistical features of the microstructural aggregate. Experimental techniques provide fundamental information, but they require suitable and generally expensive equipment and complicated and time-consuming post-processing. On the other hand, the use of reliable computer models offers

the opportunity of simulating large numbers of microstructures, helping reduce the cost of the experimental effort [2].

In the context of the analysis of heterogeneous materials, the concepts of Representative Volume Element (RVE) and Statistical Volume Element (SVE) are notions of primary importance, see e.g. Refs.[48, 49, 50, 51]. If a single microstructural *realization*[1] is considered, then it is important to determine the minimum size of the unit cell needed to attain material representativity. For polycrystalline materials, the size of the RVE can be expressed in terms of the number of grains N_g contained in the artificial microstructure. For unidirectional (UD) fibre-reinforced composites the size of the RVE is measured by the parameter δ, defined as the ratio between the length L of the side of a square unit cell and the radius r of the inclusion, typically a fibre, i.e.

$$\delta = \frac{L}{r}. \tag{35}$$

A definition of RVE can also be provided considering not only *volume* averages over individual realizations of different sizes, but also *ensemble* averages over a set of realizations of the same size, provided that a sufficient number of samples is considered [52], which suggests the concept of SVE. With this approach, the estimation of the effective properties is obtained by computing the ensemble average of the apparent properties over a collection of realizations having the same size.

In the subsequent sections, the multi-region VEM strategy adopted for computational homogenization of heterogeneous materials is described, highlighting the features of the VEM that result particularly convenient for the meshing of irregular geometries, namely the VEM ability of naturally dealing with hanging nodes and non-convex or heavily distorted mesh elements. The method has been implemented for both polycrystalline and unidirectional (UD) fibre-reinforced composite materials, which are treated separately in the next sections to better highlight the specific modelling requirements and the adopted solutions.

[1]The term *realization* is used in this work to denote the specific morphology associated to a set of randomly scattered seed points, which can identify the centroids of polycrystals generated through Voronoi tessellations or the position of the fibres in fibre-reinforced composites; in this sense, the specific morphology has a role analogous to the value assumed by a random variable.

3.1. Polycrystalline materials

The modelling strategy employed for the analysis of polycrystalline materials at the micro-scale is described in this section, starting from the method adopted for the construction of the artificial microstructure.

3.1.1. Generation of artificial polycrystalline micro-morphologies

A reliable computer representation of the polycrystalline microstructure must retain the main topological, morphological and crystallographic features of the aggregate such as number of vertices, edges and faces per grain, grain size distribution, grain shape and crystallographic orientation. Voronoi tessellations, which are analytically well defined and relatively simple to generate, have been successfully used to reproduce the main statistical features of real polycrystalline morphologies [8, 9, 22, 53] (see Fig.(2)).

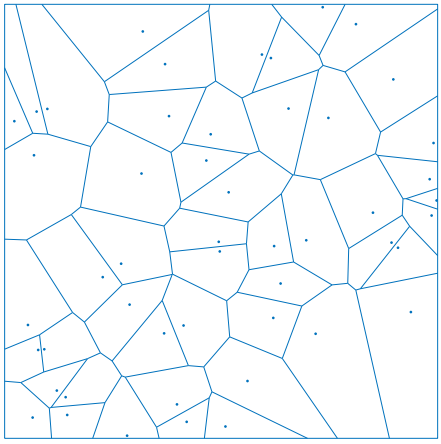

Fig. 2. Example of two-dimensional Voronoi tessellation on a square domain.

Given a bounded domain $\Omega \in \mathbb{R}^2$, its Voronoi tessellation is constructed starting from a set of n seed points $S = \{\boldsymbol{x}_i \in \Omega : i \in I_n\}$, with $I_n = \{1, 2, ..., n\}$. A Voronoi cell $\mathcal{G}_i$ having the seed $\mathbf{x}_i$ as its generator is defined as the set of points which are closer to $\mathbf{x}_i$ than to any other seed point, i.e.

$$\mathcal{G}_i = \{\mathbf{x} : \|\mathbf{x} - \mathbf{x}_i\| < \|\mathbf{x} - \mathbf{x}_j\| \; \forall j \neq i, \; j \in I_n\} \tag{36}$$

Each seed is the generator of its own Voronoi cell and all cells form a Voronoi diagram, which divides the two-dimensional space into the union of convex, non-overlapping polygons with straight edges.

The topology and morphology of the tessellation depend on the distribution of the seeds within the domain Ω. It has been shown that a Voronoi tessellation, built on a set of randomly distributed seeds, referred to as Poisson-Voronoi tessellation, possesses statistical features that make it topologically close to real polycrystalline aggregates [54]. However, randomly distributed seed points tend to generate Voronoi tessellations with a high number of highly irregular or excessively distorted grains, that are particularly challenging from the point of view of mesh preparation for subsequent numerical analysis. Various techniques have been used to produce tessellations with non-pathological grain shapes or edges, e.g. enforcing a hardcore condition on the initial distribution of seed points or by employing more sophisticated regularization procedures, addressed at avoiding an excessively refined mesh induced by the presence of small edges in the mathematically exact built tessellation [4, 22].

In the present study, two-dimensional Voronoi tessellations are used to generate artificial polycrystalline microstructures, where each Voronoi cell represents an individual grain. In order to demonstrate the ability of the Virtual Element Method to deal with mesh elements of very general polygonal shape, also generated over irregular geometries, no regularization scheme is adopted and instead a pure Poisson-Voronoi tessellation, with uniform random grain distribution and size, is used.

The tessellations have been generated using the Qhull [55] algorithm included in `MATLAB` to generate a uniform distribution inside the square domain representing the boundary of the unit cell. Since the edge length of the square domain is fixed, the only input required is the number of seed points, equal to the number of grains. Fig.(3) shows different microstructural morphologies corresponding to different numbers of grains N_g.

3.1.2. Micro-mechanical polycrystalline modelling

A linear elastic orthotropic model is used to describe the mechanical behaviour of individual crystals. The hypothesis of orthotropic material is not restrictive, since the majority of single crystal metallic and ceramic materials present a general orthotropic behaviour. For an orthotropic material in a three-dimensional framework, the linear elastic constitutive laws introduced in Eq.(2)

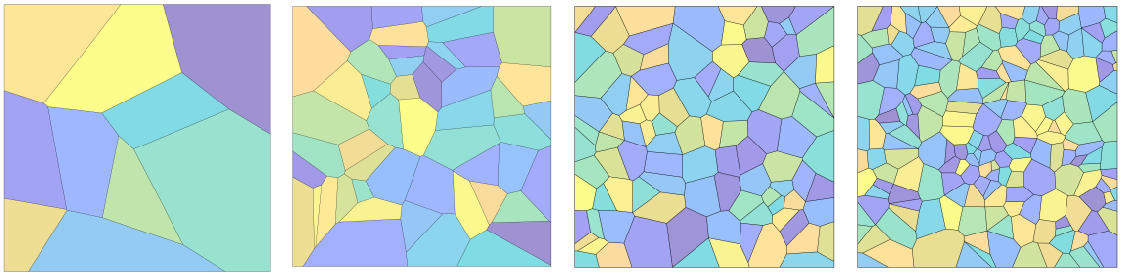

(a) (b) (c) (d)

Fig. 3. Polycrystalline morphologies with different numbers of grains: *a)* $N_g = 10$; *b)* $N_g = 50$; *c)* $N_g = 100$; *d)* $N_g = 200$.

may be written as

$$\begin{bmatrix} \sigma_{11} \\ \sigma_{22} \\ \sigma_{33} \\ \sigma_{23} \\ \sigma_{13} \\ \sigma_{12} \end{bmatrix} = \begin{bmatrix} C_{11} & C_{12} & C_{13} & 0 & 0 & 0 \\ C_{12} & C_{22} & C_{23} & 0 & 0 & 0 \\ C_{13} & C_{23} & C_{33} & 0 & 0 & 0 \\ 0 & 0 & 0 & C_{44} & 0 & 0 \\ 0 & 0 & 0 & 0 & C_{55} & 0 \\ 0 & 0 & 0 & 0 & 0 & C_{66} \end{bmatrix} \begin{bmatrix} \varepsilon_{11} \\ \varepsilon_{22} \\ \varepsilon_{33} \\ \gamma_{23} \\ \gamma_{13} \\ \gamma_{12} \end{bmatrix} \tag{37}$$

where $\gamma_{ij} = 2\varepsilon_{ij}$ for $i = 1, ...3$ and $i \neq j$.

Each grain of the microstructure is assumed to have a random spatial orientation of the principal material directions $\{1, 2, 3\}$. Although two-dimensional problems are considered in the present study, the possibility of investigating the effect of randomness of the spatial orientation of each grain on the overall behaviour of the microstructure is preserved, as explained next. Following [9], each generated grain has, randomly, one of three principal material directions that coincides with the z-axis (normal to the analysis plane). Moreover, for each grain, the angle $\theta \in [0, 2\pi)$ between the global axes x and y and the axes of the two principal material directions lying in the plane $x-y$ is also randomly generated, Fig.(4).

The artificial polycrystalline morphology generated according to the procedure explained in Sec. 3.1.1 can be considered as a multi-domain problem, in which different elastic properties and orientations are assigned to each grain. In the context of the FEM, several strategies have been used, in the literature, for the automatic generation of meshes for polycrystalline microstructures and both structured and unstructured meshes have been used [22, 56, 57].

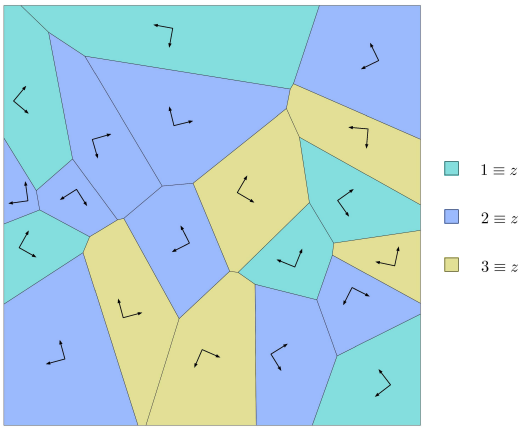

Fig. 4. Example distribution of the principal material directions within each grain. The three different colours specify which principal direction coincides with the global z-axis. The orientations in the $x - y$ plane of the other two principal material directions is represented by two black vectors.

Structured mesh are generally unable to resolve the grain boundaries, while unstructured meshes overcome this issue. However, given the morphological properties of random Voronoi tessellations, the generation of high quality conforming meshes requires a high degree of refinement that significantly increases the number of degrees of freedom.

In the present study, a multi-domain conforming meshing strategy is adopted, which takes advantage of the particular capability of the VEM of dealing with polygonal mesh elements with arbitrary number of edges as well as with hanging nodes. Each grain of the microstructure has been independently *meshed* using a Centroidal Voronoi Tessellation (CVT; not to be confused with the tessellation used to generate the morphology), which allows subdividing the often very irregular grain geometry into quite regular polygonal elements (see Fig.(5)). For this purpose, a modified version of `Polymesher` [58] is used; `Polymesher` is a mesh generator for polygonal elements written in `MATLAB`. The number of elements per grain is given as input, defined as the ratio between the grain area and the requested global mesh size.

Once all the grains have been *independently* meshed, in general, at the grain boundaries, there will be sets of collinear nodes belonging to different grains, which would induce a non-conformal mesh of the microstructure. However, since the VEM is able to deal with general polygonal elements, also presenting aligned consecutive edges, the creation of conformal meshes is conceptually straightforward and it can be attained by just adding nodes on edges shared between different

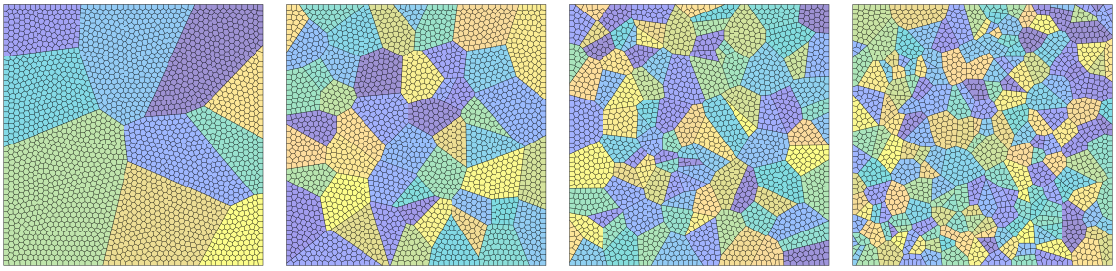

(a) (b) (c) (d)

Fig. 5. Polygonal meshes of different polycrystalline aggregates with increasing numbers of grains: *a*) $N_g = 10$; *b*) $N_g = 50$; *c*) $N_g = 100$; *d*) $N_g = 200$.

grains. Fig.(6) shows the creation of conforming meshes between adjacent grains: the presence of nodes initially hanging between contiguous grains is dealt with by transforming such nodes into vertices shared between the contiguous elements belonging to two adjacent grains. For the generic boundary polygonal element, such vertices are located between aligned consecutive edges, which are naturally dealt with by the VEM. In other words, the nodes that would be hanging in a common FEM implementations, are here treated as regular nodes, leveraging on the ability of the VEM of dealing with polygonal elements with arbitrary number of edges and also with collinear consecutive edges.

Polycrystalline microstructures generated using the described strategies have been used to perform the computational material homogenization reported in Section 4.

3.2. Unidirectional fibre-reinforced composite materials

The modelling methodology adopted for the homogenization of composite fibre-reinforced materials is described in this section. In general, reinforcing fibres may be randomly distributed within the matrix, and this can induce irregular and complex meshes. The versatility of the VEM in dealing with general polygonal elements, including non-convex or distorted elements, allows noticeable simplification of the pre-processing effort.

3.2.1. Generation of artificial composite micro-morphologies

Several algorithms have been proposed in the literature to generate microstructures of UD fibre-reinforced composite materials, see e.g. [59, 60, 61] and references therein. In the present study, artificial periodic microstructures of fibre-reinforced composites are generated as square unit

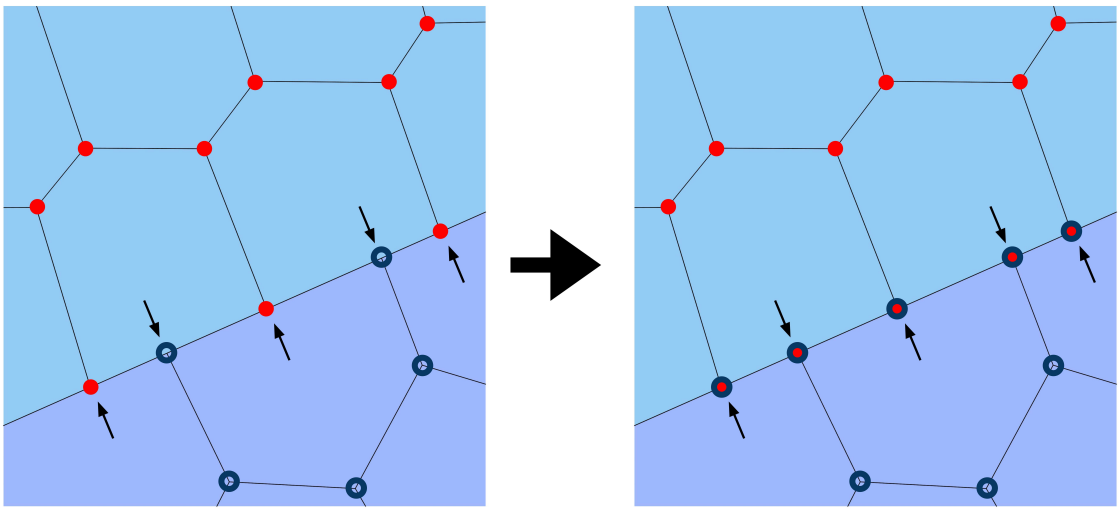

Fig. 6. Creation of conforming meshes between adjacent grains: the nodes initially hanging between contiguous grains are transformed into vertices shared between the contiguous elements belonging to two adjacent grains.

cells with random circular disk-shaped inclusions representing the fibres' transversal sections. An individual morphology is generated starting from two input parameters: the target volume fraction V_f and the size parameter δ (see Eq.(35)). The number of fibre inclusions N_f in the unit cell is given by

$$N_f = \frac{V_f \delta^2}{\pi}. \tag{38}$$

A non-overlapping condition is enforced by setting a minimum allowed distance d between the centers of the circular disk-shaped inclusions, with $d > 2r$, where r is given by Eq.(35). In order to generate a valid periodic microstructure with random fibre distribution, the following iterative procedure is adopted:

1. A random uniform set of N_f seed points is initially scattered within the squared bounding box representing the boundary of the unit cell;

2. To attain microstructural periodicity, the set of seed points is replicated within eight copies of the original box created around the original unit cell; each one of the surrounding boxes has the same size as that of the original one, so that a total of $9N_f$ points are created overall (the process is similar to the one adopted e.g. in Ref.[62]);

3. A Delaunay triangulation of the *extended domain* is generated starting from the $9N_f$ points;

4. For each edge of the triangulation, the distance between the end vertices is computed; if such length is $\leq 2r$, the vertices are moved apart along the direction identified by the edge itself of distance proportional to the original edge length;

5. The new coordinates of the original N_f points are the extracted. If in step 3, any point has been translated, the set of N_f points with the new coordinates is sent to step 2 for a new iteration; otherwise, the process is terminated.

Once a set of points respecting the non-overlapping condition is obtained, a disk-shaped inclusion can be associated to each seed; the desired periodic microstructure is then extracted by trimming the original bounding box, with circular inclusions, out of the extended domain. Some realizations obtained for different values of δ and $V_f = 0.29$ are shown in Fig.(7).

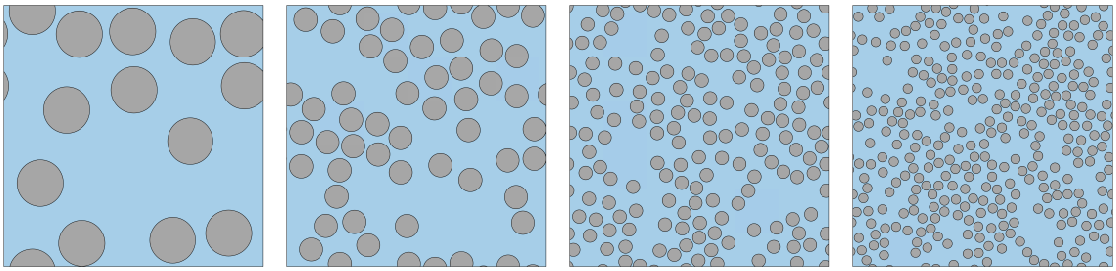

(a) (b) (c) (d)

Fig. 7. Different realizations of fibre-reinforced composite unit cells for $V_f = 0.29$ and different values of the parameter $\delta = L/r$: *a*) $\delta = 10$; *b*) $\delta = 20$; *c*) $\delta = 35$; *d*) $\delta = 50$.

3.2.2. Micro-mechanical composites modelling

Unidirectional fibre-reinforced composites can be macroscopically considered as transversely isotropic materials, whose properties emerge from the features and interplay of their constituents, i.e. from the properties of fibres, matrix, fibre-matrix interface and the ratio V_f between the volume of fibres and the total volume of the composite.

For representing the composite microstructure, a multi-domain meshing strategy is adopted that is slightly different from the one used for the polycrystalline microstructure. Still, the ability of

VEM to handle elements of very general shape is exploited. The adopted meshing strategy is based on the three following steps:

1. A conforming triangular mesh of the considered artificial micro-morphology is generated using the software `DistMesh` [63];

2. A polygonal mesh is built from the bounded Voronoi diagram generated using the centroids of the triangular mesh elements as seed points;

3. The polygonal element of the mesh obtained which intersect the fibre inclusions boundaries are trimmed so to conform to such boundaries.

The above process allows the generation of a regular polygonal discretization over the whole computational domain with the exception of the areas close to the fibre boundaries, where the ability of VEM to handle elements of arbitrary shapes, including non-convex shapes is exploited. Fig.(8) shows an example of polygonal mesh generated for a composite unit cell sample and the detail in the inset on the right shows how irregular polygonal elements may appear in proximity of the inclusions boundaries; the capability of the VEM to address irregular, distorted or non-convex elements allows to retain meshes that would require regularization or further treatment otherwise.

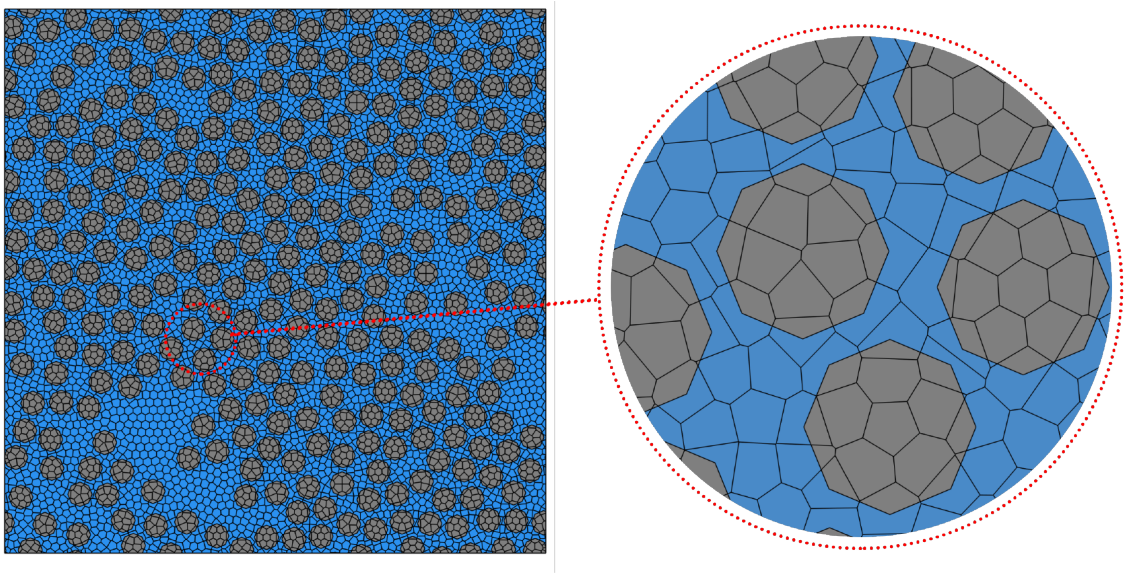

Fig. 8. Generation of a polygonal mesh for a composite unit cell morphology with $V_f = 0.44$ and $\delta = 40$ (*left*).

Indeed, the use of VEM may also simplify the implementation of straightforward regularization schemes. An example is provided in Fig.(9): the meshing of a fibre-reinforced composite through the operations summarised above may induce the presence of polygonal elements of size comparatively too small with respect to the average mesh size, represented as the blue elements in Fig.(9a); in this case, it may be useful to *absorb* such small entities within contiguous elements, the red ones in Fig.(9a-9b). While such "absorption" operation would require nodes/edges shifting in standard FEM, it can be performed using VEM by just retaining the external polygonal edges of the absorbing/absorbed element couples, as shown in (9b). This simple strategy, discussed here as an example of the flexibility allowed by the VEM in dealing with meshing, noticeably reduces the number of small elements in general composite unit cells, also reducing the possibility of artefacts in the local fields; however, the cost of the subsequent computational analysis is generally little affected, unless very large numbers of such small elements are present.

4. Computational homogenization tests

This section describes the numerical tests performed to validate the developed homogenization procedure and the reliability of the Virtual Element Method with respect to such application. The purpose of the numerical tests is the estimation of the effective transverse elastic properties of polycrystalline and unidirectional fibre-reinforced composite materials. The obtained numerical results are compared with available analytical bounds.

For each microstructural sample, assuming plane strain conditions, the apparent transverse elastic properties are calculated from the solution of three different boundary value problems, differing only in the prescribed set of boundary conditions. Kinematic uniform boundary conditions, i.e. linear displacements boundary conditions are enforced at all external nodes of the considered microstructure. Such enforced boundary displacements correspond to a macro-strain $\bar{\mathbf{\Gamma}}$. More specifically, if a reference system $x-y$ with the axes aligned with the external edges of the unite cell is adopted, the three different sets of displacement boundary conditions correspond to: a) a uniaxial direct macro-strain along the x direction; b) a uniaxial direct macro-strain along the y direction; c) a pure shear macro-strain acting to modify the angle between the axes xy. The enforced displacement micro-BCs are related to the macroscopic strain by the relation

$$\bar{u}_i = \bar{\Gamma}_{ij} x_j \quad \forall \mathbf{x} \in \partial\Omega. \tag{39}$$

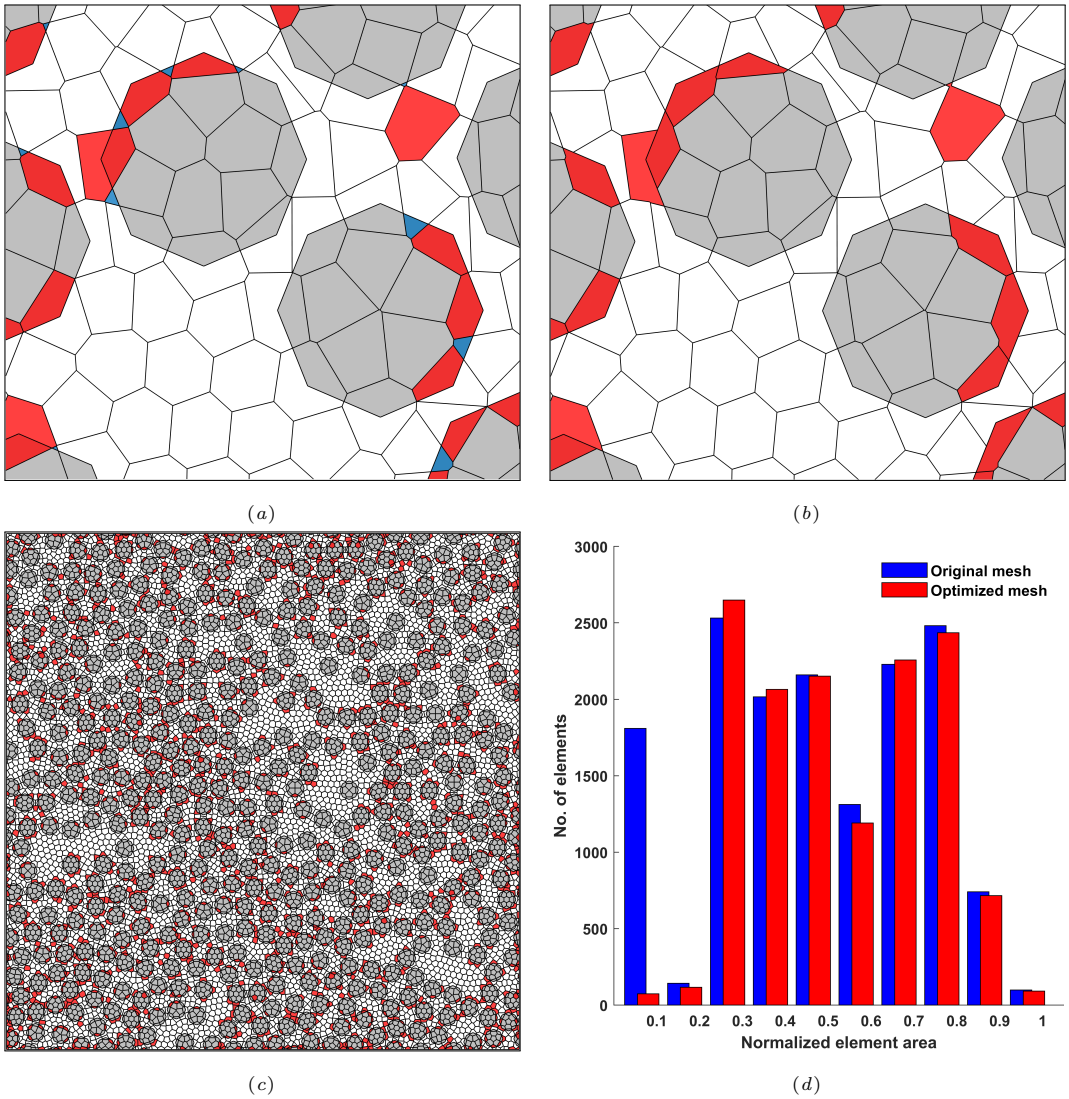

Fig. 9. A simple VEM-based regularization scheme: a) elements considerably smaller than the average mesh size may be present in the mesh of the composite fibre-reinforced unit cell (blue in the online version of the paper); b) the small elements can be *absorbed* within contiguous elements of larger size (red in the online version of the manuscript); with VEM such operation is performed by simply creating larger polygonal elements bounded by the external edges of the absorbing/absorbed element couple. In unit cells with large numbers of fibres, e.g. the one shown in (c) with 477 fibres, $\delta = 50$ and $V_f = 0.44$, the regularization scheme noticeably reduces the presence of small elements, as shown by the histogram in (d).

The relation between macro-stress and macro-strain is given by:

$$\Sigma_{ij} = \hat{\mathbb{C}}_{ijkl}\Gamma_{kl} \tag{40}$$

where $\hat{\mathbb{C}}$ is the apparent macroscopic fourth-order elastic tensor, while Σ_{ij} are the components of the macroscopic stress tensor, which can be computed upon solution of the micro baoundary value problem by the volume average of the local micro stress tensor over the domain of the RVE, i.e.

$$\Sigma_{ij} = \frac{1}{|\Omega|}\int_{\Omega} \sigma_{ij}(\mathbf{x})\mathrm{d}\Omega. \tag{41}$$

In Voigt notation, the apparent macroscopic elastic tensor $\hat{\mathbb{C}}$ is expressed through the apparent stiffness matrix $\hat{\boldsymbol{C}}$ whose components can be determined column-wise from the solution of the three linearly independent boundary value problems mentioned above. Once an estimate of the apparent stiffness matrix is available, the apparent elastic modula can be readily estimated.

4.1. Computational homogenization of FCC polycrystals

The determination of the macroscopic properties of materials presenting microscopic cubic symmetry has been previously addressed in the literature, see e.g. Ref.[64]. Numerical simulations are performed in order to estimate the effective transverse elastic properties, namely the macroscopic isotropic Young's modulus $\hat{E}$ and shear modulus $\hat{G}$, for three different polycrystalline materials presenting cubic symmetry at crystal level: copper, gold and nickel. In the case of materials with cubic symmetry, such as FCC metals, the specification about the grains orientation, as mentioned in Section 3.1.1, is unnecessary and the three principal axes are equivalent. Grains with cubic symmetry present only three distinct elastic constants C_{11}, C_{12} and C_{44} and the reduced stiffness matrix for plain strain $\boldsymbol{C}$ reads

$$\boldsymbol{C} = \begin{bmatrix} C_{11} & C_{12} & 0 \\ C_{12} & C_{11} & 0 \\ 0 & 0 & C_{44} \end{bmatrix}. \tag{42}$$

The elastic constants for the three selected materials are summarized in Table(1), as taken from Ref.[64].

For each material, aggregates with $N_g = 10, 20, 50, 100, 200$ grains have been tested. For given material and number of grains, 50 different realizations have been generated and analyzed. Each realization differs from the others in terms of both geometry and grains orientation. Table(2)

reports the minimum, the average and the maximum number of degrees of freedoms, related to the number of grains, in the analyzed polycrystalline microstructures.

The homogenization is performed following the procedure employed in Ref.[64]. For a macroscopically isotropic aggregate, the range of the Young and shear effective moduli is bounded by a lower (Reuss) bound and an upper (Voigt) bound. Such limits are also referred in the literature as first order bounds. The Reuss [65] lower bound is obtained by assuming that all the grains undergo uniform stress, while the Voigt [66] upper bound is obtained by assuming that all the grains undergo uniform strain. Since a two-dimensional model is being considered, the bounds are computed by averaging the single crystal plain strain reduced stiffness matrix over all possible orientations of the random angle θ formed between the material direction 1 and the lower horizontal edge of the square unit cell, as shown e.g. in Ref.[67].

The obtained numerical results, in terms of the effective Young's modulus $\hat{E}$ and shear modulus $\hat{G}$, are shown in Fig.(10). The Reuss and Voigt bounds are also shown for comparison purpose. The effective properties are estimated as the ensemble average over realizations containing the same number of grains. It is noticed how, as the number of grains per realization increases, the scatter of the apparent properties reduces. When realizations with $N_g = 200$ are considered, the apparent moduli always fall within the first order bounds.

4.2. Computational homogenization of fibre-reinforced composites

Two of the unidirectional fibre-reinforced composite materials considered in Ref.[68] are selected for the numerical tests on composite unit cells. The first composite, here labeled COMP1, is made of AS4 carbon fibres embedded in $3501-6$ epoxy matrix. The second composite, here labeled COMP2, is made of *Silenka* E-glass 1200 tex fibres embedded in MY750/HY917/DY063 epoxy matrix. The fibre volume fractions considered in the performed tests are $V_f = 0.22$, $V_f = 0.29$, $V_f = 0.36$ and $V_f = 0.44$.

	C_{11}	C_{12}	C_{44}
Copper	168	121	75
Gold	185	158	40
Nickel	251	150	124

Table 1: Single crystal elastic constants used for the analysed materials from Ref.[64]; the values are given in [GPa].

	N_g	10	20	50	100	200
n_{dof}	*Min*	9982	9976	9966	9938	9886
	Average	9995	9994	9988	9975	9942
	Max	10006	10012	10020	10022	9986

Table 2: Minimum, average and maximum number of DOFs for the analyzed polycrystalline aggregates.

The axis (1) is parallel to the fibres and it is normal to the (2-3) plane, in which the 2D unit cell lies. The mechanical properties of the constituents, themselves isotropic in the (2-3) plane, are given in Table(3) in terms of transverse Young modulus E_{22} and transverse shear modulus G_{23}.

Table 3: Mechanical properties for the matrix and fibres of COMP1 and COMP2, as taken from Ref.[68].

Mechanical Properties	E_{22} [GPa]	G_{23} [GPa]
AS4 carbon fibres	15	7
3501-6 epoxy matrix	4.2	1.567
Silenka E-Glass 1200 tex fibres	74	30.8
MY750/HY917/DY063 epoxy matrix	3.35	1.24

A unidirectional fibre-reinforced composite lamina is macroscopically transversely isotropic, so that only two elastic modula are needed to completely characterize the transverse behaviour in the plane of isotropy (2-3). In this study, the results of the numerical tests are given in terms of the plain strain bulk modulus K_{23} and the shear modulus G_{23}.

The minimal RVE size for unidirectional fibre-reinforced composites similar to those considered here has been investigated in Ref.[69], where it was found that, when the purpose of the analysis is the estimation of the effective properties, a minimum size parameter of $\delta \geq 30$ is required. In this study, the convergence of the effective properties is assessed in the range $10 \leq \delta \leq 50$.

Figs.(11-12) show, for both composite materials and for each considered value of the volume fraction V_f, the average and the scatter range of the computed elastic properties as a function of the unit cell size, as expressed by δ. The average is computed over ensembles of 50 realizations for each value of δ. It can be observed that, for both considered materials and for $\delta \geq 30$, there is no appreciable variation in the values of either the average elastic modula or the scatter, which

confirms convergence of the effective properties (please note the tight scale used in the graphs).

Figs.(13-14) show the numerical predictions about the computed transverse mechanical properties K_{23} and G_{23} versus the fibre-volume fraction V_f at $\delta = 50$. The Voigt and Reuss bounds and the Hashin-Hill bounds [48, 70] for the effective elastic modula are also shown for comparison purpose. The obtained numerical estimates are in agreement with the theoretical predictions.

Table (4) shows the minimum, average and maximum number of degrees of freedoms, in the analyzed composite microstructures, for $V_f = 0.22$ and at different values of the size parameter δ.

5. Conclusions

A lowest-order Virtual Element framework for computational materials homogenization has been developed and it has been applied to both polycrystalline materials and unidirectional fibre-reinforced composites. General polycrystalline Voronoi microstructures have been analysed addressing the occurrence of hanging nodes at the interface between independently meshed contiguous grains through the ability of VEM of dealing with elements with aligned edges. The ability of VEM of addressing non-convex polygonal element, on the other hand, has been employed in the analysis of general composite fibre-reinforced morphologies, obtained from the random scattering of fibres with circular sections. In summary, the study shows how the capability of the Virtual Element Method to deal with very general polygonal mesh elements, including non-convex and highly distorted elements, can be profitably exploited to relax the requirements on the mesh quality that may hinder the automatic analysis of micro-morphologies presenting complex or highly statistically varying features, commonly met in computational materials micro-mechanics and homogenization, where materials microstructures are often generated resorting to stochastic algorithms.

Table 4: Minimum, average and maximum number of DOFs for the analyzed composite microstructures for $V_f = 0.22$.

	N_g	10	15	20	25	30	35	40	45	50
	Min	1836	3700	6604	10328	14670	19750	25828	32438	39842
n_{dof}	*Average*	1932	3772	6711	10349	14838	19906	26018	32651	40117
	Max	1984	3856	6810	10470	15022	20098	26174	32868	40354

Data availability

The raw/processed data required to reproduce these findings cannot be shared at this time due to technical or time limitations.

References

References

[1] S. Nemat-Nasser, M. Hori, Micromechanics: overall properties of heterogeneous materials, Vol. 37, Elsevier, 2013.

[2] T. I. Zohdi, P. Wriggers, An introduction to computational micromechanics, Vol. 20 of Lecture Notes in Applied and Computational Mechanics, Springer-Verlag Berlin Heidelberg, 2005. doi:10.1007/978-3-540-32360-0.

[3] F. Roters, P. Eisenlohr, L. Hantcherli, D. Tjahjanto, T. Bieler, D. Raabe, Overview of constitutive laws, kinematics, homogenization and multiscale methods in crystal plasticity finite-element modeling: Theory, experiments, applications, Acta Materialia 58 (4) (2010) 1152 – 1211. doi:https://doi.org/10.1016/j.actamat.2009.10.058.
URL http://www.sciencedirect.com/science/article/pii/S1359645409007617

[4] V. Gulizzi, A. Milazzo, I. Benedetti, An enhanced grain-boundary framework for computational homogenization and micro-cracking simulations of polycrystalline materials, Computational Mechanics 56 (4) (2015) 631–651.

[5] I. Benedetti, V. Gulizzi, V. Mallardo, A grain boundary formulation for crystal plasticity, International Journal of Plasticity 83 (2016) 202 – 224. doi:https://doi.org/10.1016/j.ijplas.2016.04.010.
URL http://www.sciencedirect.com/science/article/pii/S0749641916300596

[6] A. A. Gusev, P. J. Hine, I. M. Ward, Fiber packing and elastic properties of a transversely random unidirectional glass/epoxy composite, Composites Science and Technology 60 (4) (2000) 535 – 541. doi:https://doi.org/10.1016/S0266-3538(99)00152-9.
URL http://www.sciencedirect.com/science/article/pii/S0266353899001529

[7] A. Melro, P. Camanho, S. Pinho, Influence of geometrical parameters on the elastic response of unidirectional composite materials, Composite Structures 94 (11) (2012) 3223 – 3231. doi:https://doi.org/10.1016/j.compstruct.2012.05.004.
URL http://www.sciencedirect.com/science/article/pii/S0263822312002139

[8] F. Barbe, L. Decker, D. Jeulin, G. Cailletaud, Intergranular and intragranular behavior of polycrystalline aggregates. part 1: F.e. model, International Journal of Plasticity 17 (4) (2001) 513 – 536. doi:https://doi.org/10.1016/S0749-6419(00)00061-9.
URL http://www.sciencedirect.com/science/article/pii/S0749641900000619

[9] H. D. Espinosa, P. D. Zavattieri, A grain level model for the study of failure initiation and evolution in polycrystalline brittle materials. part i: Theory and numerical implementation, Mechanics of Materials 35 (3) (2003) 333 – 364. doi:https://doi.org/10.1016/S0167-6636(02)00285-5.
URL http://www.sciencedirect.com/science/article/pii/S0167663602002855

[10] Y. Huang, K. K. Jin, S. K. Ha, Effects of fiber arrangement on mechanical behavior of unidirectional composites, Journal of composite materials 42 (18) (2008) 1851–1871.

[11] A. Melro, P. Camanho, F. A. Pires, S. Pinho, Micromechanical analysis of polymer composites reinforced by unidirectional fibres: Part i – constitutive modelling, International Journal of Solids and Structures 50 (11) (2013) 1897 – 1905. doi:https://doi.org/10.1016/j.ijsolstr.2013.02.009.
URL http://www.sciencedirect.com/science/article/pii/S0020768313000747

[12] A. Melro, P. Camanho, F. A. Pires, S. Pinho, Micromechanical analysis of polymer composites reinforced by unidirectional fibres: Part ii – micromechanical analyses, International Journal of Solids and Structures 50 (11) (2013) 1906 – 1915. doi:https://doi.org/10.1016/j.ijsolstr.2013.02.007.
URL http://www.sciencedirect.com/science/article/pii/S0020768313000723

[13] N. Sukumar, D. Srolovitz, T. Baker, J.-H. Prévost, Brittle fracture in polycrystalline microstructures with the extended finite element method, International Journal for Numerical Methods in Engineering 56 (14) (2003) 2015–2037.

[14] G. Stefanou, D. Savvas, M. Papadrakakis, Stochastic finite element analysis of composite structures based on material microstructure, Composite Structures 132 (2015) 384 – 392. doi:https://doi.org/10.1016/j.compstruct.2015.05.044.
URL http://www.sciencedirect.com/science/article/pii/S0263822315004183

[15] G. Geraci, M. Aliabadi, Micromechanical modelling of cohesive thermoelastic cracking in orthotropic polycrystalline materials, Computer Methods in Applied Mechanics and Engineering 339 (2018) 567 – 590. doi:https://doi.org/10.1016/j.cma.2018.05.011.
URL http://www.sciencedirect.com/science/article/pii/S0045782518302548

[16] V. Gulizzi, C. Rycroft, I. Benedetti, Modelling intergranular and transgranular micro-cracking in polycrystalline materials, Computer Methods in Applied Mechanics and Engineering 329 (2018) 168 – 194. doi:https://doi.org/10.1016/j.cma.2017.10.005.
URL http://www.sciencedirect.com/science/article/pii/S0045782517306746

[17] I. Benedetti, V. Gulizzi, A. Milazzo, Grain-boundary modelling of hydrogen assisted intergranular stress corrosion cracking, Mechanics of Materials 117 (2018) 137 – 151. doi:https://doi.org/10.1016/j.mechmat.2017.11.001.
URL http://www.sciencedirect.com/science/article/pii/S0167663617305276

[18] I. Benedetti, V. Gulizzi, A grain-scale model for high-cycle fatigue degradation in polycrystalline materials, International Journal of Fatigue 116 (2018) 90 – 105. doi:https://doi.org/10.1016/j.ijfatigue.2018.06.010.
URL http://www.sciencedirect.com/science/article/pii/S0142112318302287

[19] T. D. Dang, B. V. Sankar, Meshless local petrov-galerkin micromechanical analysis of periodic composites including shear loadings, COMPUTER MODELING IN ENGINEERING AND SCIENCES 26 (3) (2008) 169.

[20] P. Wen, M. Aliabadi, Elastic moduli of woven fabric composite by meshless local petrov-galerkin(mlpg) method, Computer Modeling in Engineering & Sciences(CMES) 61 (2) (2010) 133–154.

[21] H. Qing, L. Mishnaevsky, Unidirectional high fiber content composites: Automatic 3d fe model generation and damage simulation, Computational Materials Science 47 (2) (2009) 548 – 555.

585 doi:https://doi.org/10.1016/j.commatsci.2009.09.023.
URL http://www.sciencedirect.com/science/article/pii/S092702560900367X

[22] R. Quey, P. Dawson, F. Barbe, Large-scale 3d random polycrystals for the finite element method: Generation, meshing and remeshing, Computer Methods in Applied Mechanics and Engineering 200 (17) (2011) 1729 – 1745. doi:https://doi.org/10.1016/j.cma.2011.01.
590 002.
URL http://www.sciencedirect.com/science/article/pii/S004578251100003X

[23] L. Beirão da Veiga, F. Brezzi, A. Cangiani, G. Manzini, L. D. Marini, A. Russo, Basic principles of virtual element methods, Mathematical Models and Methods in Applied Sciences 23 (01) (2013) 199–214.

595 [24] L. Beirão da Veiga, F. Brezzi, L. D. Marini, A. Russo, The hitchhiker's guide to the virtual element method, Mathematical models and methods in applied sciences 24 (08) (2014) 1541–1573.

[25] L. Beirão da Veiga, F. Brezzi, L. D. Marini, Virtual elements for linear elasticity problems, SIAM Journal on Numerical Analysis 51 (2) (2013) 794–812.

600 [26] A. L. Gain, C. Talischi, G. H. Paulino, On the virtual element method for three-dimensional linear elasticity problems on arbitrary polyhedral meshes, Computer Methods in Applied Mechanics and Engineering 282 (2014) 132–160.

[27] E. Artioli, L. B. Da Veiga, C. Lovadina, E. Sacco, Arbitrary order 2d virtual elements for polygonal meshes: Part i, elastic problem, Computational Mechanics 60 (3) (2017) 355–377.

605 [28] L. Beirão da Veiga, C. Lovadina, D. Mora, A virtual element method for elastic and inelastic problems on polytope meshes, Computer Methods in Applied Mechanics and Engineering 295 (2015) 327 – 346. doi:https://doi.org/10.1016/j.cma.2015.07.013.
URL http://www.sciencedirect.com/science/article/pii/S004578251500225X

[29] E. Artioli, L. B. Da Veiga, C. Lovadina, E. Sacco, Arbitrary order 2d virtual elements for
610 polygonal meshes: Part ii, inelastic problem, Computational Mechanics 60 (4) (2017) 643–657.

[30] P. Wriggers, B. D. Reddy, W. Rust, B. Hudobivnik, Efficient virtual element formulations for compressible and incompressible finite deformations, Computational Mechanics 60 (2) (2017)

253–268. doi:10.1007/s00466-017-1405-4.
URL https://doi.org/10.1007/s00466-017-1405-4

[31] H. Chi, L. B. da Veiga, G. Paulino, Some basic formulations of the virtual element method (vem) for finite deformations, Computer Methods in Applied Mechanics and Engineering 318 (2017) 148 – 192. doi:https://doi.org/10.1016/j.cma.2016.12.020.
URL http://www.sciencedirect.com/science/article/pii/S0045782516309094

[32] P. Wriggers, W. Rust, B. Reddy, A virtual element method for contact, Computational Mechanics 58 (6) (2016) 1039–1050.

[33] A. L. Gain, G. H. Paulino, L. S. Duarte, I. F. Menezes, Topology optimization using polytopes, Computer Methods in Applied Mechanics and Engineering 293 (2015) 411–430.

[34] P. F. Antonietti, M. Bruggi, S. Scacchi, M. Verani, On the virtual element method for topology optimization on polygonal meshes: A numerical study, Computers & Mathematics with Applications 74 (5) (2017) 1091–1109.

[35] L. Beirão da Veiga, F. Brezzi, F. Dassi, L. Marini, A. Russo, Virtual element approximation of 2d magnetostatic problems, Computer Methods in Applied Mechanics and Engineering 327 (2017) 173–195.

[36] L. Beirão da Veiga, F. Brezzi, F. Dassi, L. Marini, A. Russo, Lowest order virtual element approximation of magnetostatic problems, Computer Methods in Applied Mechanics and Engineering 332 (2018) 343–362.

[37] O. Andersen, H. M. Nilsen, X. Raynaud, Virtual element method for geomechanical simulations of reservoir models, Computational Geosciences 21 (5) (2017) 877–893. doi:10.1007/s10596-017-9636-1.
URL https://doi.org/10.1007/s10596-017-9636-1

[38] M. F. Benedetto, A. Caggiano, G. Etse, Virtual elements and zero thickness interface-based approach for fracture analysis of heterogeneous materials, Computer Methods in Applied Mechanics and Engineering 338 (2018) 41–67.

[39] V. M. Nguyen-Thanh, X. Zhuang, H. Nguyen-Xuan, T. Rabczuk, P. Wriggers, A virtual element method for 2d linear elastic fracture analysis, Computer Methods in Applied Mechanics and Engineering.

[40] F. Brezzi, L. D. Marini, Virtual element methods for plate bending problems, Computer Methods in Applied Mechanics and Engineering 253 (2013) 455 – 462. doi:https://doi.org/10.1016/j.cma.2012.09.012.
URL http://www.sciencedirect.com/science/article/pii/S0045782512002940

[41] L. Beirão da Veiga, D. Mora, G. Rivera, Virtual elements for a shear-deflection formulation of reissner-mindlin plates, Mathematics of Computation 88, 315 (2019) 149–178. arXiv:1710.07330.

[42] E. Artioli, Asymptotic homogenization of fibre-reinforced composites: a virtual element method approach, Meccanica 53 (6) (2018) 1187–1201.

[43] E. Artioli, S. Marfia, E. Sacco, High-order virtual element method for the homogenization of long fiber nonlinear composites, Computer Methods in Applied Mechanics and Engineering 341 (2018) 571–585.

[44] P. Wriggers, B. Hudobivnik, J. Schröder, Finite and virtual element formulations for large strain anisotropic material with inextensive fibers, in: Multiscale Modeling of Heterogeneous Structures, Springer, 2018, pp. 205–231.

[45] M. Pingaro, E. Reccia, P. Trovalusci, R. Masiani, Fast statistical homogenization procedure (fshp) for particle random composites using virtual element method, Computational Mechanics 64 (1) (2019) 197–210. doi:10.1007/s00466-018-1665-7.
URL https://doi.org/10.1007/s00466-018-1665-7

[46] M. Marino, B. Hudobivnik, P. Wriggers, Computational homogenization of polycrystalline materials with the virtual element method, Computer Methods in Applied Mechanics and Engineering 355 (2019) 349 – 372. doi:https://doi.org/10.1016/j.cma.2019.06.004.
URL http://www.sciencedirect.com/science/article/pii/S0045782519303445

[47] N. Sukumar, A. Tabarraei, Conforming polygonal finite elements, International Journal for Numerical Methods in Engineering 61 (12) (2004) 2045–2066.

[48] R. Hill, Elastic properties of reinforced solids: Some theoretical principles, Journal of the Mechanics and Physics of Solids 11 (5) (1963) 357 – 372. doi:https://doi.org/10.1016/0022-5096(63)90036-X.
URL http://www.sciencedirect.com/science/article/pii/002250966390036X

[49] Z. Hashin, Analysis of composite materials—a survey, Journal of Applied Mechanics 50 (3) (1983) 481–505.

[50] M. Ostoja-Starzewski, Microstructural randomness versus representative volume element in thermomechanics, Journal of Applied Mechanics 69 (1) (2002) 25–35.

[51] I. Gitman, H. Askes, L. Sluys, Representative volume: existence and size determination, Engineering fracture mechanics 74 (16) (2007) 2518–2534.

[52] T. Kanit, S. Forest, I. Galliet, V. Mounoury, D. Jeulin, Determination of the size of the representative volume element for random composites: statistical and numerical approach, International Journal of Solids and Structures 40 (13) (2003) 3647 – 3679. doi:https://doi.org/10.1016/S0020-7683(03)00143-4.
URL http://www.sciencedirect.com/science/article/pii/S0020768303001434

[53] I. Benedetti, M. H. Aliabadi, A three-dimensional cohesive-frictional grain-boundary micromechanical model for intergranular degradation and failure in polycrystalline materials, Computer Methods in Applied Mechanics and Engineering 265 (2013) 36–62.

[54] S. Kumar, S. K. Kurtz, Simulation of material microstructure using a 3d voronoi tesselation: Calculation of effective thermal expansion coefficient of polycrystalline materials, Acta Metallurgica et Materialia 42 (12) (1994) 3917 – 3927. doi:https://doi.org/10.1016/0956-7151(94)90170-8.
URL http://www.sciencedirect.com/science/article/pii/0956715194901708

[55] C. B. Barber, D. D. P., H. H. T., The quickhull algorithm for convex hulls, ACM Trans. Math. Softw. 22 (1996) 469–483.

[56] S. Ghosh, K. Lee, S. Moorthy, Multiple scale analysis of heterogeneous elastic structures using homogenization theory and voronoi cell finite element method, International Journal of Solids and Structures 32 (1) (1995) 27 – 62. doi:https://doi.org/10.1016/0020-7683(94)

00097-G.
URL http://www.sciencedirect.com/science/article/pii/002076839400097G

[57] F. Fritzen, T. Böhlke, E. Schnack, Periodic three-dimensional mesh generation for crystalline aggregates based on voronoi tessellations, Computational Mechanics 43 (5) (2009) 701–713.

[58] C. Talischi, G. H. Paulino, A. Pereira, I. F. M. Menezes, Polymesher: a general-purpose mesh generator for polygonal elements written in matlab, Structural and Multidisciplinary Optimization 45 (3) (2012) 309–328. doi:10.1007/s00158-011-0706-z.
URL https://doi.org/10.1007/s00158-011-0706-z

[59] A. Melro, P. Camanho, S. Pinho, Generation of random distribution of fibres in long-fibre reinforced composites, Composites Science and Technology 68 (9) (2008) 2092 – 2102. doi:https://doi.org/10.1016/j.compscitech.2008.03.013.
URL http://www.sciencedirect.com/science/article/pii/S0266353808001048

[60] G. Catalanotti, On the generation of rve-based models of composites reinforced with long fibres or spherical particles, Composite Structures 138 (2016) 84 – 95. doi:https://doi.org/10.1016/j.compstruct.2015.11.039.
URL http://www.sciencedirect.com/science/article/pii/S0263822315010429

[61] M. Pathan, V. Tagarielli, S. Patsias, P. Baiz-Villafranca, A new algorithm to generate representative volume elements of composites with cylindrical or spherical fillers, Composites Part B: Engineering 110 (2017) 267 – 278. doi:https://doi.org/10.1016/j.compositesb.2016.10.078.
URL http://www.sciencedirect.com/science/article/pii/S1359836816313725

[62] I. Benedetti, M. Aliabadi, Multiscale modeling of polycrystalline materials: A boundary element approach to material degradation and fracture, Computer Methods in Applied Mechanics and Engineering 289 (2015) 429 – 453. doi:https://doi.org/10.1016/j.cma.2015.02.018.
URL http://www.sciencedirect.com/science/article/pii/S0045782515000675

[63] P. Persson, G. Strang, A simple mesh generator in matlab, SIAM Review 46 (2) (2004) 329–345. arXiv:https://doi.org/10.1137/S0036144503429121, doi:10.1137/S0036144503429121.
URL https://doi.org/10.1137/S0036144503429121

[64] I. Benedetti, M. H. Aliabadi, A three-dimensional grain boundary formulation for microstructural modeling of polycrystalline materials, Computational Materials Science 67 (2013) 249–260.

[65] A. Reuss, Berechnung der fließgrenze von mischkristallen auf grund der plastizitätsbedingung für einkristalle., ZAMM-Journal of Applied Mathematics and Mechanics/Zeitschrift für Angewandte Mathematik und Mechanik 9 (1) (1929) 49–58.

[66] W. Voigt, Lehrbuch der kristallphysik, Vol. 962, Teubner Leipzig, 1928.

[67] R. Mullen, R. Ballarini, Y. Yin, A. Heuer, Monte carlo simulation of effective elastic constants of polycrystalline thin films, Acta Materialia 45 (6) (1997) 2247 – 2255. doi:https://doi.org/10.1016/S1359-6454(96)00366-7.
URL http://www.sciencedirect.com/science/article/pii/S1359645496003667

[68] P. Soden, M. Hinton, A. Kaddour, Lamina properties, lay-up configurations and loading conditions for a range of fibre-reinforced composite laminates, Composites Science and Technology 58 (7) (1998) 1011 – 1022. doi:https://doi.org/10.1016/S0266-3538(98)00078-5.
URL http://www.sciencedirect.com/science/article/pii/S0266353898000785

[69] D. Trias, J. Costa, A. Turon, J. Hurtado, Determination of the critical size of a statistical representative volume element (srve) for carbon reinforced polymers, Acta Materialia 54 (13) (2006) 3471 – 3484, selected Papers from the Meeting "Micromechanics and Microstructure Evolution: Modeling, Simulation and Experiments" held in Madrid/Spain, 11–16 September 2005. doi:https://doi.org/10.1016/j.actamat.2006.03.042.
URL http://www.sciencedirect.com/science/article/pii/S1359645406002497

[70] Z. Hashin, On elastic behaviour of fibre reinforced materials of arbitrary transverse phase geometry, Journal of the Mechanics and Physics of Solids 13 (3) (1965) 119 – 134. doi:https://doi.org/10.1016/0022-5096(65)90015-3.
URL http://www.sciencedirect.com/science/article/pii/0022509665900153

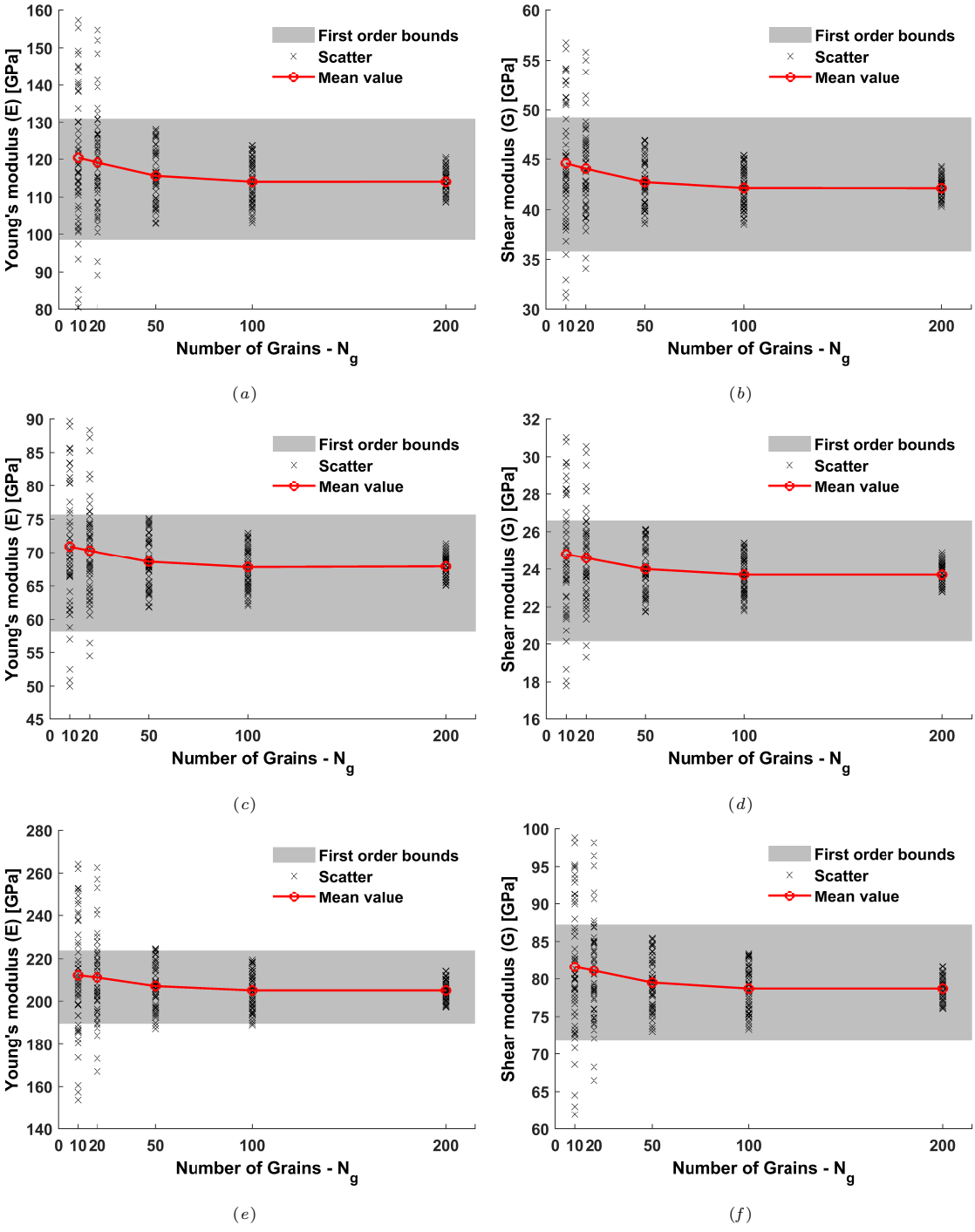

Fig. 10. Computed effective Young's modulus E and shear modulus G for polycrystalline aggregates of copper (a-b), gold (c-d), nickel (e-f).

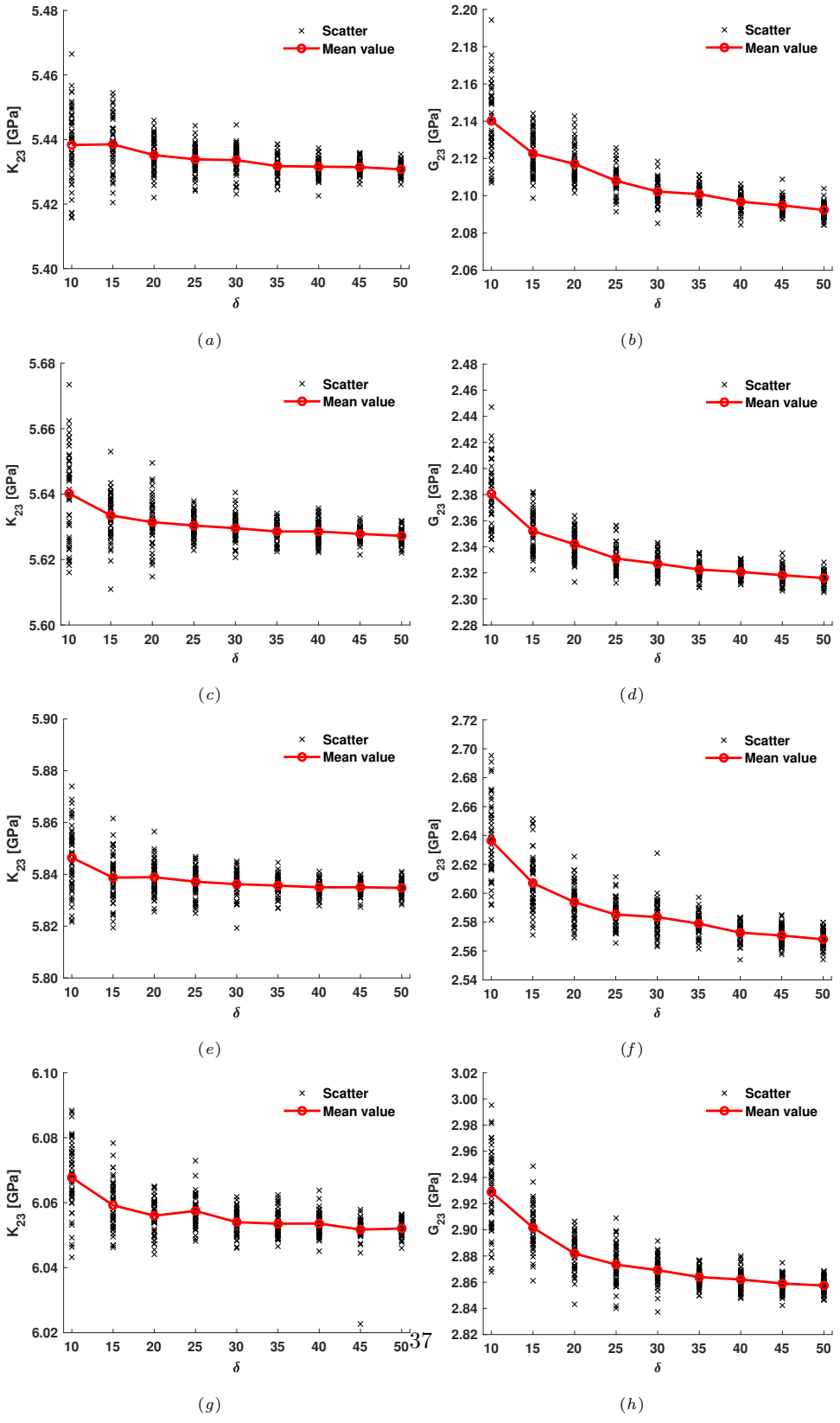

Fig. 11. Computed effective transverse elastic properties as a function of δ for different values of V_f for COMP1: $V_f = 0.22$ (a-b); $V_f = 0.29$ (c-d); $V_f = 0.36$ (e-f); $V_f = 0.44$ (g-h).

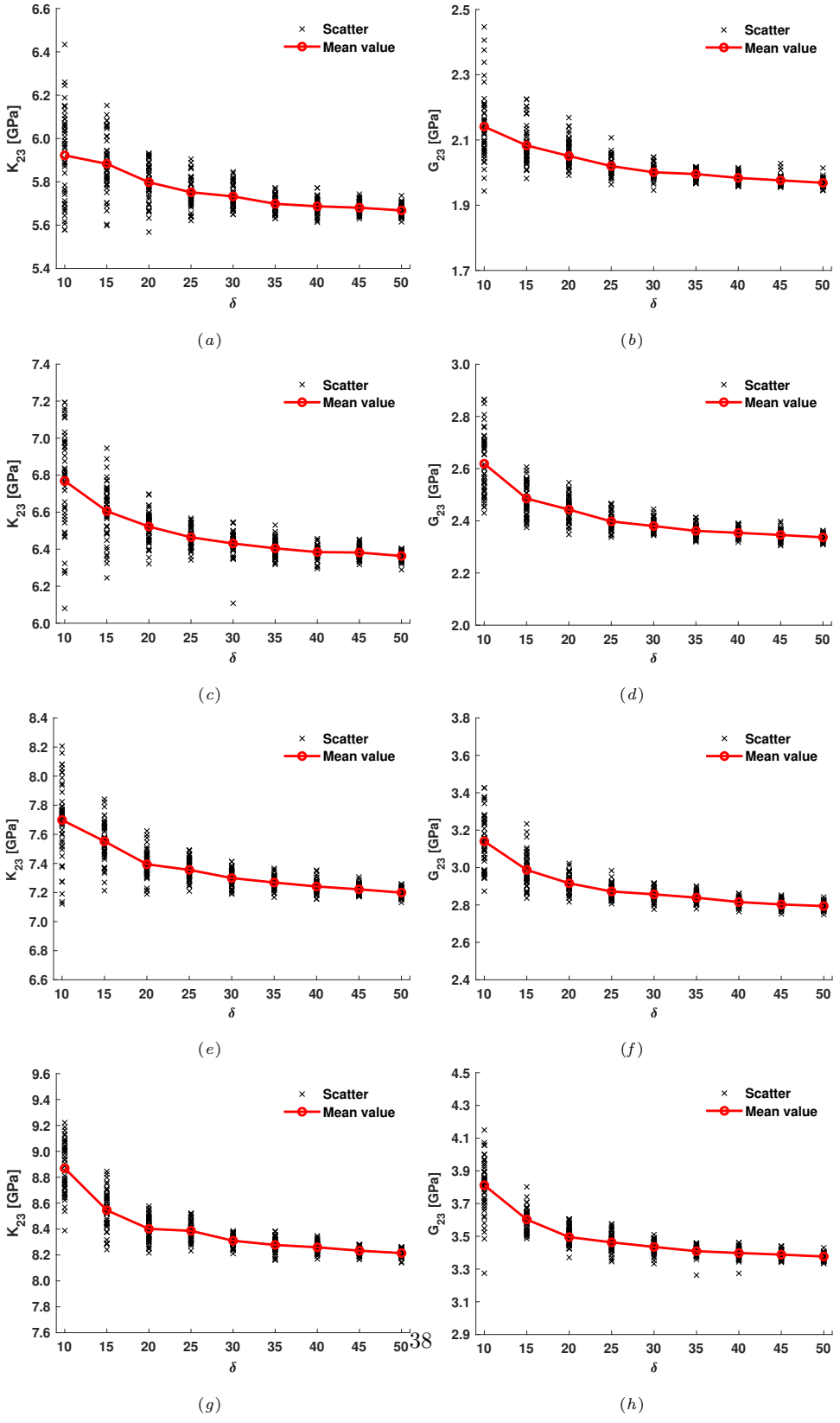

Fig. 12. Computed effective transverse elastic properties as a function of δ for different values of V_f for COMP2: $V_f = 0.22$ (a-b); $V_f = 0.29$ (c-d); $V_f = 0.36$ (e-f); $V_f = 0.44$ (g-h).

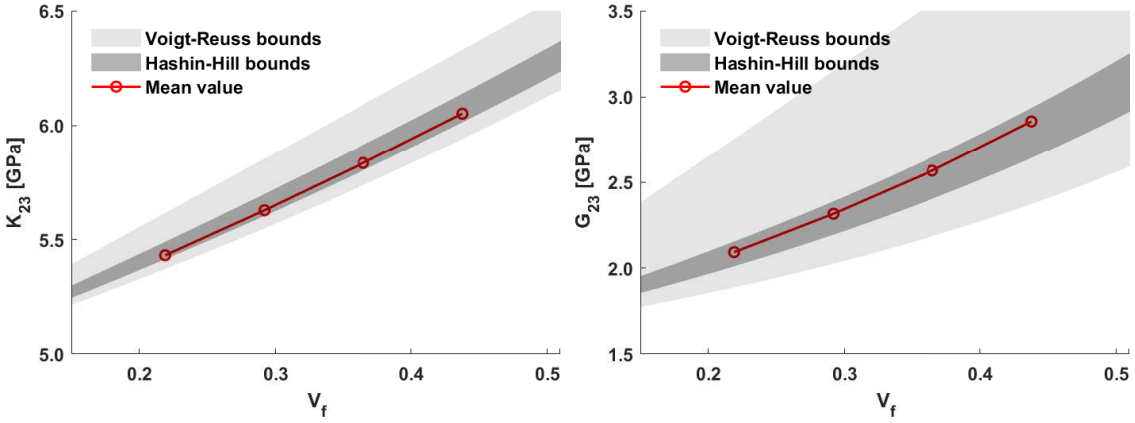

(a) (b)

Fig. 13. Computed transverse elastic properties and Hashin-Hill bounds as a function of the volume fraction V_f for COMP1 and $\delta = 50$.

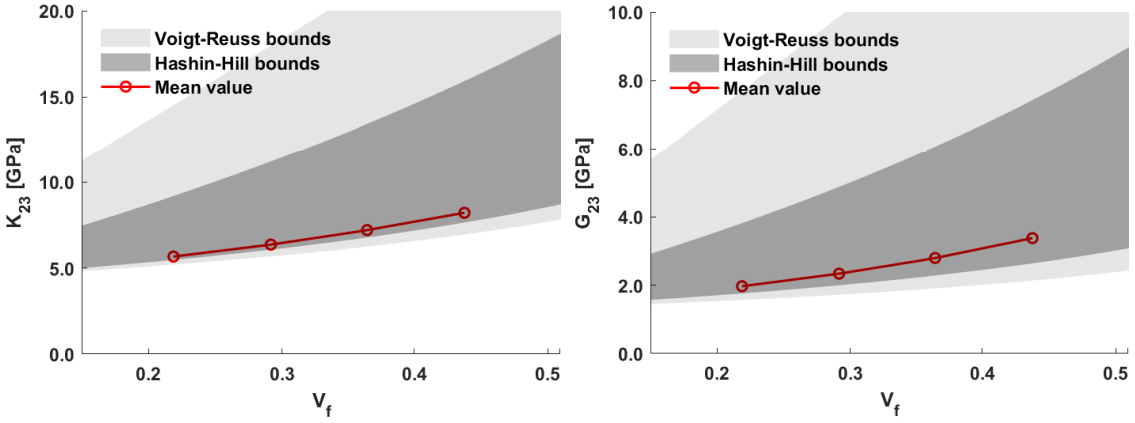

(a) (b)

Fig. 14. Computed transverse elastic properties and Hashin-Hill bounds as a function of the volume fraction V_f for COMP2 and $\delta = 50$.